Science Advances
AAAS

advances.sciencemag.org/cgi/content/full/5/8/eaax2476/DC1

Supplementary Materials for

Combinatorial morphogenetic and mechanical cues to mimic bone development for defect repair

S. Herberg, A. M. McDermott, P. N. Dang, D. S. Alt, R. Tang, J. H. Dawahare, D. Varghai, J.-Y. Shin, A. McMillan, A. D. Dikina, F. He, Y. B. Lee, Y. Cheng, K. Umemori, P. C. Wong, H. Park, J. D. Boerckel*, E. Alsberg*

*Corresponding author. Email: boerckel@pennmedicine.upenn.edu (J.D.B.); ealsberg@uic.edu (E.A.)

Published 28 August 2019, *Sci. Adv.* **5**, eaax2476 (2019)
DOI: 10.1126/sciadv.aax2476

This PDF file includes:

Supplementary Materials

Supplementary Figures

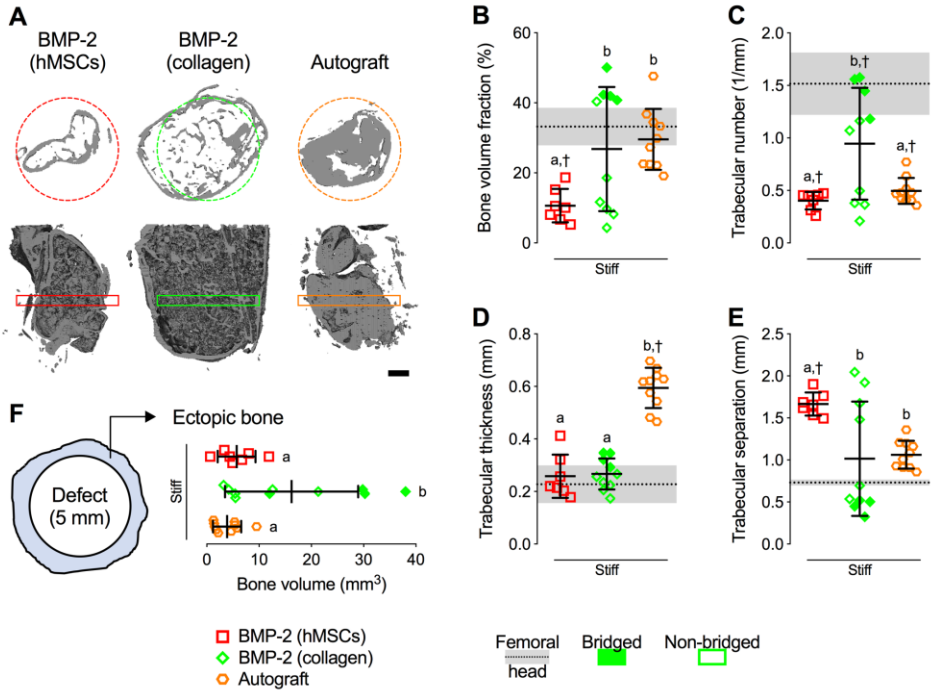

Fig. S1. Effects of BMP-2–primed engineered mesenchymal condensations and routine clinical therapies on new bone quantity and architecture in the absence of mechanical cues. (**A**) Representative 3-D microCT defect reconstructions of mid-shaft transverse (top) and sagittal (bottom) sections at week 12, selected based on mean bone volume. Dashed circles show 5 mm defect region. Rectangular boxes illustrate transverse cutting planes. Scale bar, 1 mm. (**B**) Morphometry analysis of bone volume fraction, (**C**) trabecular number, (**D**) trabecular thickness, (**E**) trabecular separation, shown with native femoral head properties (N = 3; dotted lines with gray shading: mean ± SD; $^{\dagger}p<0.05$ vs. femoral head), and (**F**) ectopic bone formation (i.e., bone extending beyond the 5-mm defect diameter) at week 12 (N = 7-10 per group). Individual data points shown with mean ± SD. Comparisons between groups were evaluated by two-way ANOVA with Tukey's post-hoc tests. Repeated significance indicator letters (a,b,c) signify $p > 0.05$, while groups with distinct indicators signify $p < 0.05$.

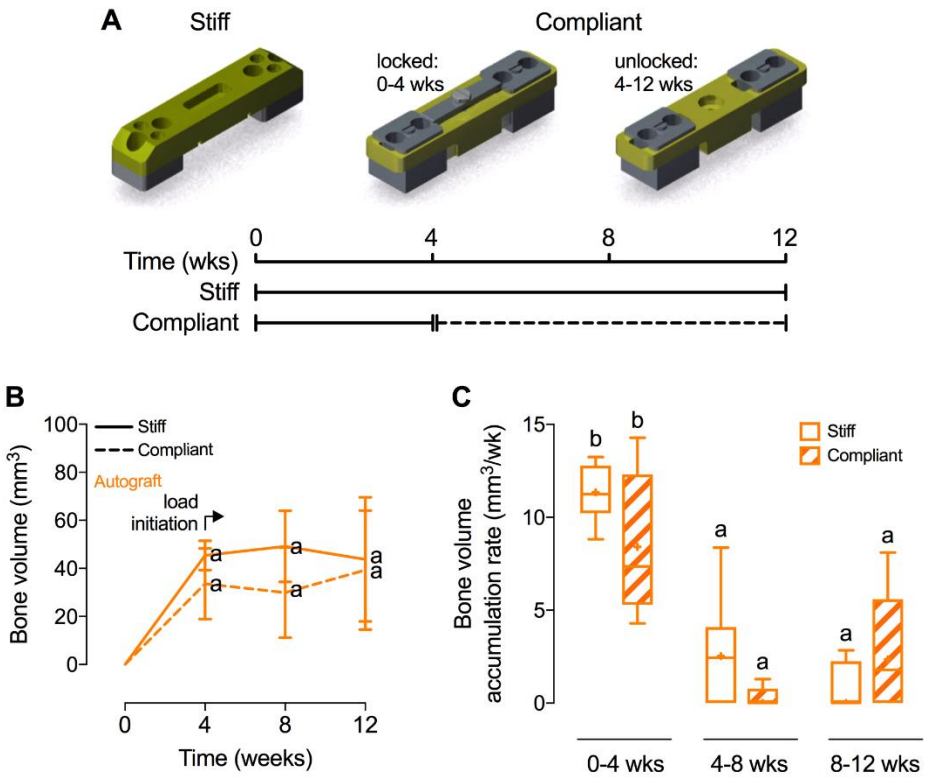

Fig. S2. Effects of morselized autografts and in vivo mechanical loading on longitudinal bone formation and bone accumulation rate. (**A**) Stiff and compliant fixation plate configurations for dynamic control of ambulatory load transfer, and loading timeline with compliant plate unlocking at week 4. (**B**) Longitudinal quantification of bone volume at weeks 4, 8, and 12 by *in vivo* microCT (N = 6-8 per group). (**C**) Bone volume accumulation rate, defined as bone volume accrual over each 4-week interval. Data shown with mean ± SD. Box plots display median as horizontal line, mean as +, inter-quartile range as boxes, and min/max range as whiskers. Comparisons between groups were evaluated by two-way ANOVA with Tukey's post-hoc tests. Repeated significance indicator letters (a,b,c) signify $p > 0.05$, while groups with distinct indicators signify $p < 0.05$ at each time point.

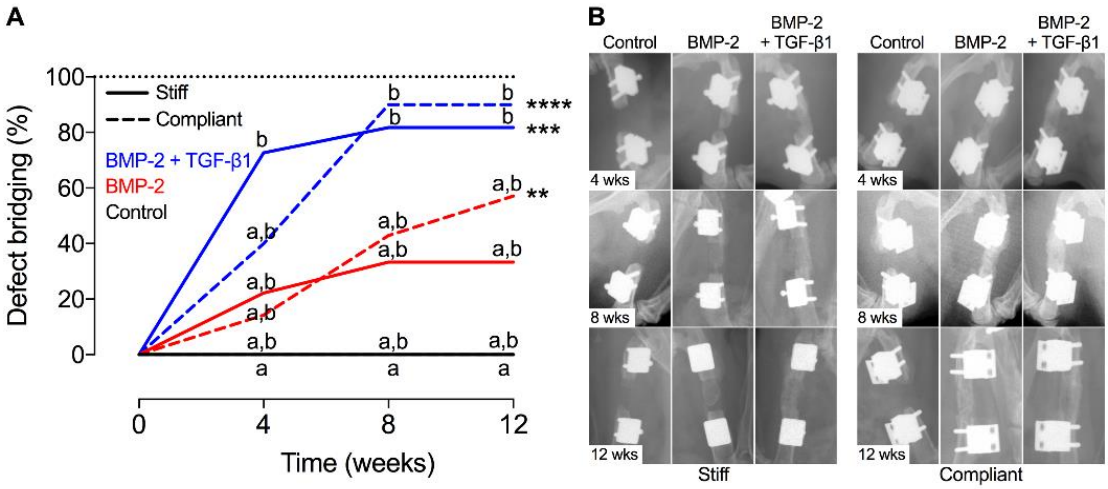

Fig. S3. Effects of morphogen priming of engineered mesenchymal condensations and in vivo mechanical loading on defect bridging. (**A**) Longitudinal determination of defect bridging by *in vivo* radiography, defined as mineral fully traversing the defect (N = 4-11 per group). (**B**) Representative radiography images at 4, 8 and 12 weeks showing defect bridging per group over time, selected based on mean bone volume at week 12 (Fig. 3). Significance of trend was analyzed by chi-square test (**p<0.01, ***p<0.001, ****p<0.0001). Differences between groups were determined by chi-square test at each time point with Bonferroni correction (p<0.01, correction factor of 5. Repeated significance indicator letters (a,b,c) signify p > 0.05, while groups with distinct indicators signify p < 0.05.

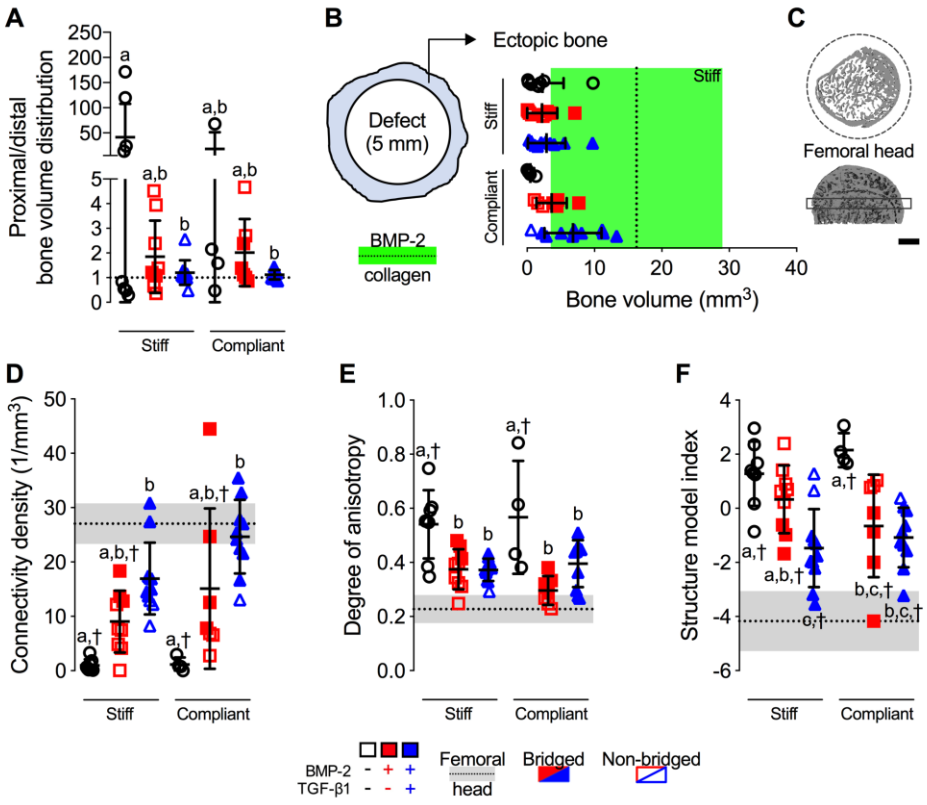

Fig. S4. Effects of morphogen priming of engineered mesenchymal condensations and in vivo mechanical loading on new bone distribution and architecture. (**A**) Morphometry analysis of proximal vs. distal bone volume distribution (N = 4-11 per group; $p<0.05$), and (**B**) ectopic bone formation (i.e., bone extending beyond the 5-mm defect diameter) shown with BMP-2 soaked on collagen data (N = 9; dotted line with green shading: mean ± SD). (**C**) Representative 3-D microCT reconstructions of native femoral head transverse (top) and sagittal (bottom) sections, selected based on mean bone volume. Dashed circles show 5 mm defect region. Rectangular box illustrates transverse cutting plane. Scale bar, 1 mm. (**D**) Morphometry analysis of connectivity density, (**E**) degree of anisotropy, and (**F**) structure model index within the defect region (N = 4-11 per group), shown with native femoral head properties (N = 3; dotted lines with gray shading: mean ± SD; $^{\dagger}p<0.05$ vs. femoral head). Individual data points shown with mean ± SD. Comparisons between groups were evaluated by two-way ANOVA with Tukey's post-hoc tests. Repeated significance indicator letters (a,b,c) signify $p > 0.05$, while groups with distinct indicators signify $p < 0.05$.

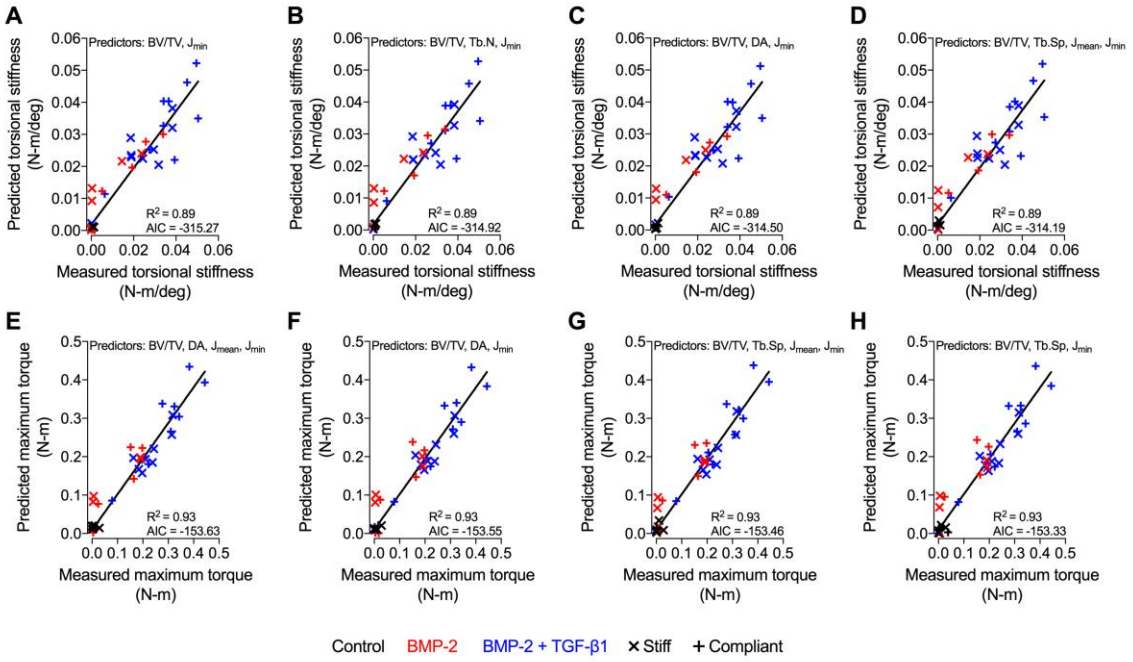

Fig. S5. Best subset analysis of mechanical testing data. Best subsets regression analysis of the top 5 models with selection made by minimization of Akaike's Information Criterion (AIC). Predictive models of (**A**-**D**) torsional stiffness and (**E**-**H**) maximum torque at failure were composed of combinations of bone volume fraction (BV/TV), trabecular number (Tb.N), trabecular separation (Tb.Sp), minimum pMOI (J_{min}), mean pMOI (J_{mean}), and degree of anisotropy (DA). Type II regression was used to determine correlations (R^2) between predicted and measured values.

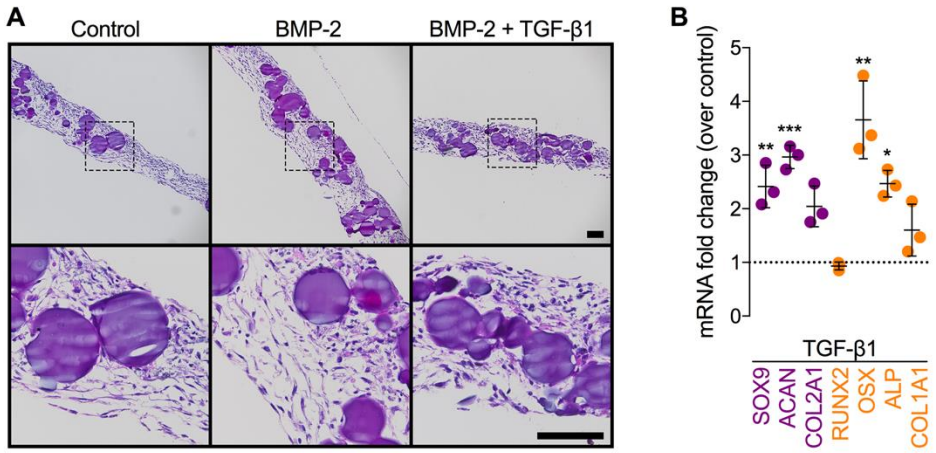

Fig. S6. Effects of morphogen priming of engineered mesenchymal condensations on in vitro chondrogenic lineage specification at the time of implantation. (**A**) Histological H&E staining of representative microparticle-containing hMSC sheets at the time of implantation (2 days; N = 3 per group). Scale bars, 100 μm (10x: top; 40x: bottom, magnification of dotted squares). (**B**) Normalized mRNA fold-change over control of key chondrogenic or osteogenic markers in TGF-β1-only loaded hMSC sheets by qRT-PCR (N = 3 per group; *p<0.05, **p<0.01, ***p<0.001 vs. control). Individual data points shown with mean ± SD. Analyzed by unpaired two-tailed Student's *t* test.

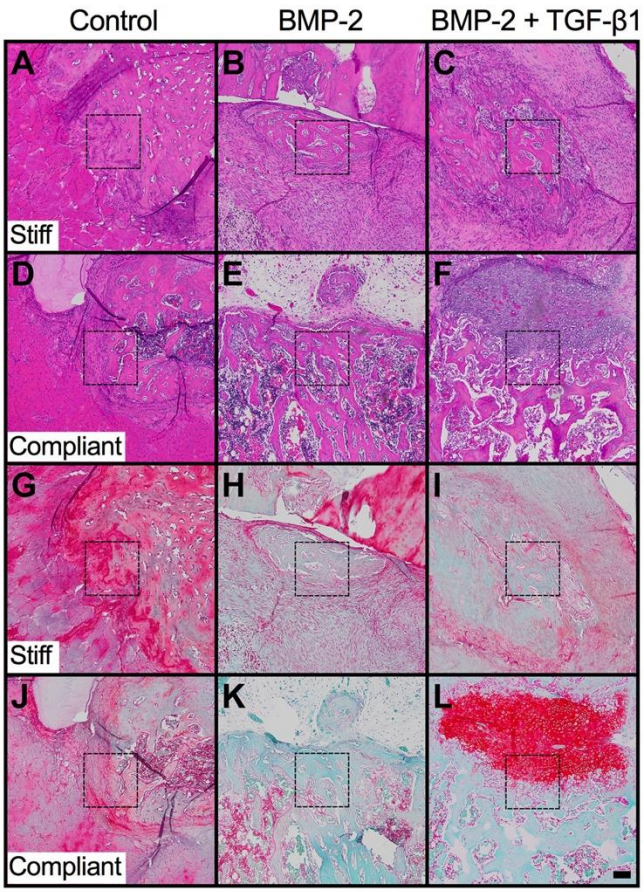

Fig. S7. Effects of morphogen priming of engineered mesenchymal condensations and in vivo mechanical loading on tissue-level bone regeneration at 4 weeks. (**A**-**F**) Representative histological H&E and (**G**-**L**) Safranin-O/Fast green staining of defect tissue at week 4, selected based on mean bone volume. Scale bar, 100 μm (10x; dotted squares show areas used in 40x images in Fig. 4A,B).

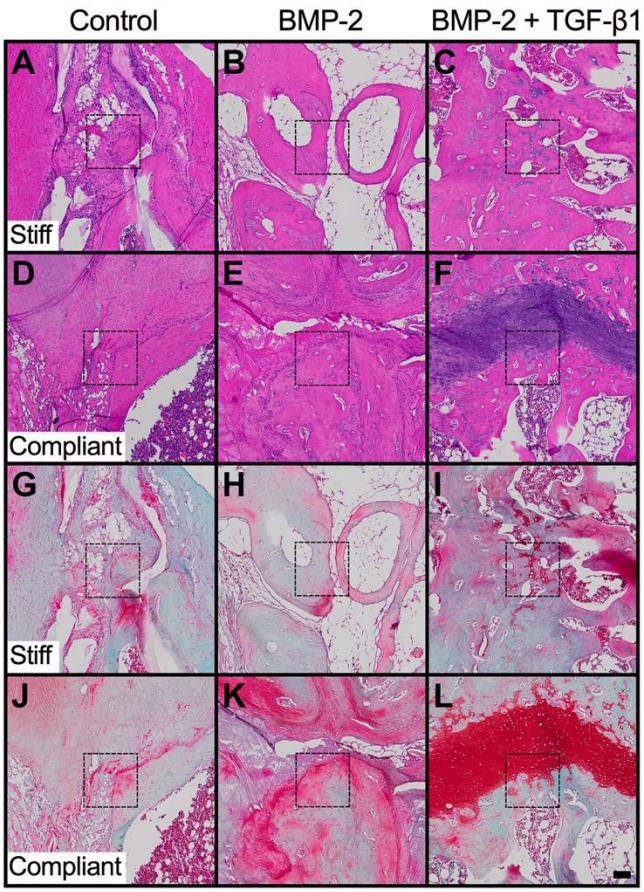

Fig. S8. Effects of morphogen priming of engineered mesenchymal condensations and in vivo mechanical loading on tissue-level bone regeneration at 12 weeks. (**A**-**F**) Representative histological H&E and (**G**-**L**) Safranin-O/Fast green staining of defect tissue at week 12, selected based on mean bone volume. Scale bar, 100 μm (10x; dotted squares show areas used in 40x images in Fig. 4A,B).

Supplementary Tables

Table S1. Oligonucleotide primer sequences for qRT-PCR.

Gene	Sequence (5'-3')		Accession number
SOX9	Fwd	CACACAGCTCACTCGACCTTG	NM_000346.3
	Rev	TTCGGTTATTTTTAGGATCATCTCG	
ACAN	Fwd	TGCGGGTCAACAGTGCCTATC	NM_001135.3
	Rev	CACGATGCCTTTCACCACGAC	
COL2A1	Fwd	GGAAACTTTGCTGCCCAGATG	NM_001844.4
	Rev	TCACCAGGTTCACCAGGATTGC	
RUNX2	Fwd	ACAGAACCACAAGTGCGGTGCAA	NM_001015051.3
	Rev	TGGCTGGTAGTGACCTGCGGA	
ALP	Fwd	CCACGTCTTCACATTTGGTG	NM_000478.4
	Rev	GCAGTGAAGGGCTTCTTGTC	
COL1A1	Fwd	GATGGATTCCAGTTCGAGTATG	NM_000088.3
	Rev	GTTTGGGTTGCTTGTCTGTTTG	
OSX	Fwd	TGGCTAGGTGGTGGGCAGGG	NM_001173467.2
	Rev	TGGGCAGCTGGGGGTTCAGT	
BMPRIA	Fwd	CAGAGATTGGAATCCGCCTGC	NM_004329.2
	Rev	ATCGGGCCGTGCGATCTT	
BMPRIB	Fwd	GCAAGCCTGCCATAAGTGAG	NM_001203.2
	Rev	CACAGGCAACCCAGAGTCAT	
BMPRII	Fwd	CTGCAAATGGCCAAGCATGT	NM_001204.6
	Rev	ATGGTTGTAGCAGTGCCTCC	
TGFBRI	Fwd	ACCCTGCCTAGTGCAAGTTAC	NM_001130916.2
	Rev	AAGCCAAGTTTTCACCCCCA	
TGFBRII	Fwd	GTTGGCGAGGAGTTTCCTGTT	NM_001024847.2
	Rev	GTCCTATTACAGCTGGGGCA	
GAPDH	Fwd	GGGGCTGGCATTGCCCTCAA	NM_002046.5
	Rev	GGCTGGTGGTCCAGGGGTCT	